JOURNAL OF VIROLOGY, Nov. 2001, p. 10815–10828 Vol. 75, No. 22
0022-538X/01/$04.00+0 DOI: 10.1128/JVI.75.22.10815–10828.2001

C Terminus of Infectious Bursal Disease Virus Major Capsid Protein VP2 Is Involved in Definition of the T Number for Capsid Assembly

JOSÉ R. CASTÓN,[1] JORGE L. MARTÍNEZ-TORRECUADRADA,[2] ANTONIO MARAVER,[3] ELEUTERIO LOMBARDO,[3] JOSÉ F. RODRÍGUEZ,[3] J. IGNACIO CASAL,[2] AND JOSÉ L. CARRASCOSA[1]*

Departments of Structure of Macromolecules[1] and Molecular and Cellular Biology,[3] Centro Nacional de Biotecnología, CSIC, Campus Universidad Autónoma de Madrid, 28049 Madrid, and Ingenasa, 28037 Madrid,[2] Spain

Received 25 April 2001/Accepted 31 July 2001

Infectious bursal disease virus **(IBDV), a member of the *Birnaviridae* family, is a double-stranded RNA virus. The IBDV capsid is formed by two major structural proteins, VP2 and VP3, which assemble to form a T=13 markedly nonspherical capsid. During viral infection, VP2 is initially synthesized as a precursor, called VPX, whose C end is proteolytically processed to the mature form during capsid assembly. We have computed three-dimensional maps of IBDV capsid and virus-like particles built up by VP2 alone by using electron cryomicroscopy and image-processing techniques. The IBDV single-shelled capsid is characterized by the presence of 260 protruding trimers on the outer surface. Five classes of trimers can be distinguished according to their different local environments. When VP2 is expressed alone in insect cells, dodecahedral particles form spontaneously; these may be assembled into larger, fragile icosahedral capsids built up by 12 dodecahedral capsids. Each dodecahedral capsid is an empty T=1 shell composed of 20 trimeric clusters of VP2. Structural comparison between IBDV capsids and capsids consisting of VP2 alone allowed the determination of the major capsid protein locations and the interactions between them. Whereas VP2 forms the outer protruding trimers, VP3 is found as trimers on the inner surface and may be responsible for stabilizing functions. Since elimination of the C-terminal region of VPX is correlated with the assembly of T=1 capsids, this domain might be involved (either alone or in cooperation with VP3) in the induction of different conformations of VP2 during capsid morphogenesis.**

Infectious bursal disease virus (IBDV) is the prototype member of the *Avibirnavirus* genus in the *Birnaviridae* family (44) and an important pathogen of chickens, accounting for important economic losses in the poultry industry worldwide and representing a major hazard for several species of wild birds (27). During the past decade there have been outbreaks of highly virulent strains against which classical vaccines were not protective (61, 77). Improvement in the control of the disease will be obtained only through further understanding of IBDV molecular biology, including viral structure.

The IBDV genome is formed by two double-stranded RNA (dsRNA) segments of 3.2 kb (segment A) and 2.8 kb (segment B) (35, 38). Segment A contains two partially overlapping open reading frames (ORFs). The first ORF encodes the nonstructural VP5 protein (17 kDa), whose functional properties are not yet clear, although it is important in virus release and dissemination (49, 60). The second ORF codes for a 110-kDa polyprotein that is autoproteolytically cleaved, yielding three proteins: VPX (~48 kDa), VP3 (32 kDa), and VP4 (28 kDa) (Fig. 1A). A major proportion of VPX (also designated pVP2) is further proteolytically processed to VP2 (41 kDa) (48, 59). Biochemical analysis of purified capsids from virions revealed that VP2 and VP3 are the major structural proteins in the mature virion (18), while VP4, a serine-lysine protease (7, 43), is involved in the proteolytic maturation of the polyprotein (22). Segment B contains an ORF that encodes VP1 (95 kDa), which is assumed to be the RNA-dependent RNA polymerase, responsible for the reactions of transcription (plus-strand or mRNA synthesis) and replication (minus-strand synthesis) (58, 73).

IBDV is a nonenveloped virus that differs from most dsRNA viruses in having a single shell. By cryoelectron microscopy and computer image reconstruction methods Böttcher et al. (8) have shown that the capsid (maximum diameter, 700 Å) is an icosahedron with 780 subunits, clustered as 260 outer trimers, arranged with a triangulation number of T=13. However, the correlation of the structural features of the capsid and the structural proteins of the virus is poorly understood.

In capsids with T>1, the protein subunits are able to adopt several different conformations depending on their different structural environments in the shell; that is, the bonding properties of subunits are not identical, and several classes of conformers exist (11). High-resolution structural studies have revealed some clues about how a capsid protein is able to know the conformation that it must adopt (see, e.g., references 5, 47, and 69), although the mechanism is still poorly understood (37). These differences are quite subtle and may be controlled by flexible regions in the protein (loops, N ends, and C ends), duplex or single-stranded RNA, metal ions, or some combination of these (36). These factors are referred to as molecular switches. Additionally, capsids with large T numbers can be

* Corresponding author. Mailing address: Departamento de Estructura de Macromoléculas, Centro Nacional de Biotecnología, CSIC, Campus UAM, Cantoblanco, 28049 Madrid, Spain. Phone: 34-91-585-4509. Fax: 34-91-585-4506. E-mail: jlcarrascosa@cnb.uam.es.

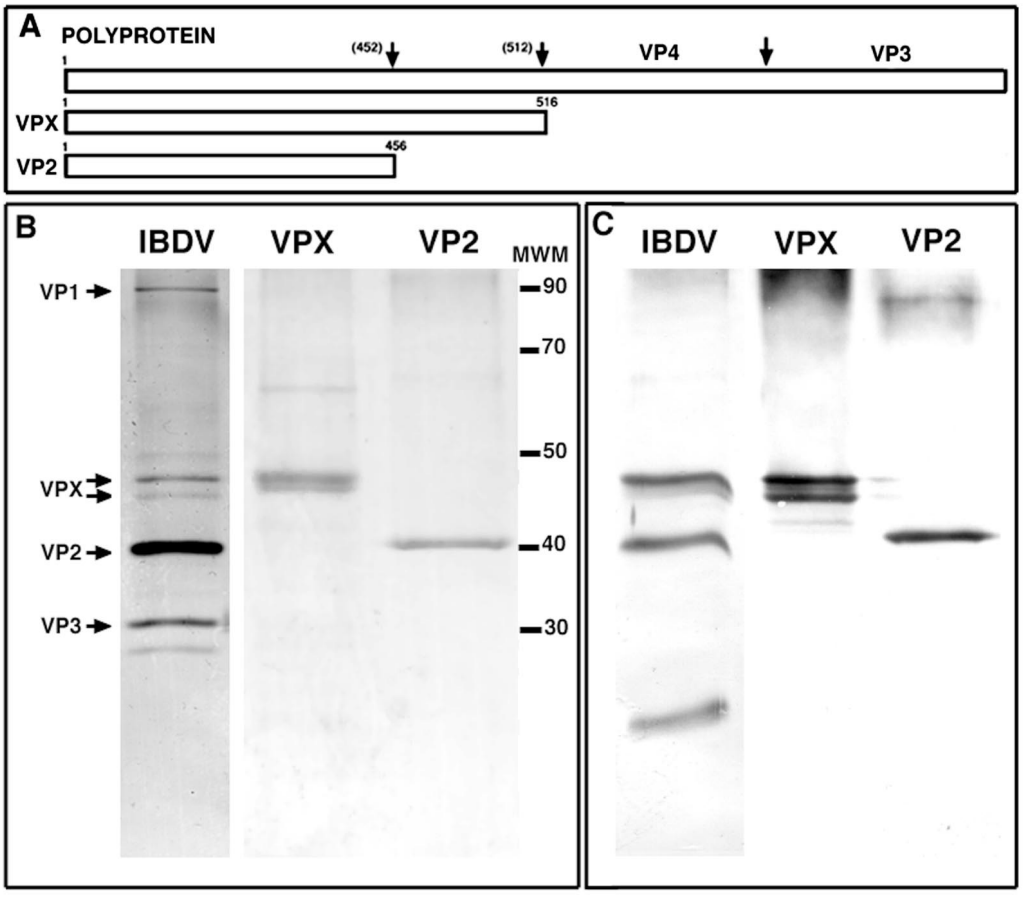

FIG. 1. Expression of VPX and VP2. (A) IBDV polyprotein structure, NH2-VPX-VP4-VP3-COOH. The recently suggested VPX–VP4 cleavage site at Ala_{512}–Ala_{513} is indicated (46, 73). The cleavage site for conversion of VPX to the mature form of VP2 is around residues 450 to 456, but it is unknown. The VPX and VP2 forms used in this work are diagrammed below the polyprotein structure. (B) Expression of VPX and VP2 by AcVPX.IBDV and AcVP2.IBDV, respectively. Purified VPX and VP2 fractions (see Materials and Methods) were subjected to SDS-PAGE (11% polyacrylamide) and detected by Coomassie blue staining. Purified IBDV particles were subjected to the same treatment with silver staining. Bands corresponding to the VP1, VPX, VP2, and VP3 proteins are indicated. Molecular weight markers (MWM), in thousands, are given on the right.(C) Detection of VPX, VP2, and IBDV virions by Western blotting with polyclonal rabbit anti-VPX serum.

achieved by one or more auxiliary proteins (scaffold, minor capsid, or enzymatic proteins) (19, 74).

We have undertaken studies of IBDV based on recombinant baculovirus and vaccinia virus systems expressing defined combinations of IBDV capsid genes in order to establish structure-function relationships and understand their architectural principles (24, 48, 51). The IBDV polyprotein expressed with the baculovirus system is processed and spontaneously assembles into different structures, e.g., rigid tubular structures, icosahedral virus-like particles (VLPs), intermediate assembly products, and tubular structures built up by VP4 (28, 51). When expressed with the vaccinia virus system, the polyprotein, either in the presence or in the absence of VP1 protein, is properly processed and forms icosahedral VLPs with a size and morphology identical to those of IBDV virions (24, 48).

In order to learn if the individual expression of the major structural proteins would regenerate any kind of particles, we have undertaken the expression of VPX, VP2, and VP3 singly and in combination (VPX and VP3; VP2 and VP3) (unpublished data). VP3 alone did not yield any type of particle (52). Here we report the different structures obtained upon expression of VPX or VP2 alone using a baculovirus expression system and their comparison with IBDV virions. We have used cryoelectron microscopy and image processing techniques to determine the three-dimensional structure of the baculovirus-expressed VP2, which forms a T=1 capsid, to a resolution of 28 Å. By comparison with the T=13 capsid from virions, we clearly demonstrate the locations of the VP2 and VP3 structural proteins in the virion capsid. Some clues about their functionality based on their locations in the T=13 capsid are discussed. Our results indicate that the C-terminal region of the VPX/VP2 capsid protein may play an important role in determining different conformations of this protein during the construction of IBDV capsids, and we discuss their implications for virion assembly.

MATERIALS AND METHODS

Virus preparation. IBDV strain Soroa, a serotype I virus, was purified by a standard protocol from chicken embryo fibroblasts infected at a multiplicity of infection of 0.1 PFU per cell (24, 48) and was stored in PES buffer [25 mM

piperazine-*N*,*N*′-bis(2-ethanesulfonic acid) (PIPES) (pH 6.2), 150 mM NaCl, 20 mM $CaCl_2$].

Construction of recombinant baculoviruses. The coding sequences of VPX and VP2 were obtained by PCR with Vent DNA polymerase (New England Biolabs) by using the recombinant plasmid pFastBac/POLY as the template (51). The oligonucleotides used were IBDV1 (5′ TTCGA*TGATCA*CGATGACAAA CCTGTCAGATC 3′) and IBDVX (5′ ACTAC*TGATCA*CCCCTTGTCGGCG GCGAGAG 3′), which cover nucleotides 1 to 1548 of ORFA1, for VPX gene amplification and IBDV1 and IBDV2 (5′ GAGAC*TGATC*ACACAGCTATC-CTCCTTATG 3′), covering nucleotides 1 to 1368 of ORFA1, for VP2 gene synthesis. *Bcl*I sites, shown in italics, were included to generate *Bam*HI-compatible ends for further cloning into the baculovirus transfer vector pAcYMI (54). The derivative plasmids, pAcYM1-VPX. IBDV and pAcYM1-VP2.IBDV, were proof sequenced. The corresponding recombinant baculoviruses, AcVPX.IBDV and AcVP2.IBDV, were obtained by standard procedures (39).

Purification of VP2 and VPX structures. Sf9 cells were infected with AcVPX. IBDV or AcVP2.IBDV at a multiplicity of infection of 1 PFU/cell. Cells were harvested at 72 h postinfection and processed as described previously (51), by purifying sedimenting material with a 25% sucrose cushion and a linear 25-to-50% sucrose gradient, both in PES buffer. Fractions containing VPX or VP2 proteins were identified by sodium dodecyl sulfate-polyacrylamide gel electrophoresis (SDS-PAGE) and Western blotting with anti-VPX rabbit serum as described elsewhere (48, 51). Enriched fractions consisting of VPX or VP2 particles were selected for structural studies and were used within 1 to 2 days of purification.

Conventional electron microscopy. Samples (5 μl) were applied to glow-discharged carbon-coated grids for 2 min. Samples were negatively stained with 2% (wt/vol) aqueous uranyl acetate. Micrographs were recorded with a JEOL 1200 EXII electron microscope operating at 100 kV at a nominal magnification of ×40,000.

Cryoelectron microscopy. Fractions containing virions or VP2 structures to be examined by cryoelectron microscopy were pooled, centrifuged at 35,000 rpm for 2 h at 4°C in an SW55 rotor (Beckman), and resuspended in PES buffer (100 to 200 μl) at 2 to 5 mg/ml. They were then dialyzed against phosphate-buffered saline (PES buffer is a "bubbling" agent under cryoelectron microscopic analysis) and diluted until a uniform distribution of particles was observed (when examined by negative staining). Drops (5 μl) of sample were applied to one side of either a holey carbon or carbon-coated grid, which was then blotted and plunged into a bath of liquid ethane (−180°C) according to established procedures (21), essentially as described previously(12). Micrographs were recorded under minimal exposure conditions so that the specimens imaged received exposures of 8 to 10 e^-/nm^2, at nominal magnifications of ×45,000 or ×40,000 on a Philips CM12 or a JEOL 1200 EXII electron microscope, respectively. Gatan 626 cryoholders operating at a temperature of about −171°C were used in both electron microscopes. Microscopes were operated at 100 kV, and images were recorded with a 1-s exposure on Kodak SO 163 electron image films, which were developed in full-strength Kodak D19 for 12 min at room temperature. In some experiments, bacteriophage T4 was vitrified and the 40.5-Å axial spacing of its tail sheath was used as an internal magnification standard (57). Micrographs were assessed for resolution and astigmatism by computer Fourier analysis and/or optical diffraction analysis, and their defocus values were estimated from the positions of the first zero of the contrast transfer function (CTF) (45). For the selected micrographs analyzed, the first zero was around 26 $Å^{-1}$.

Image analysis. Micrographs were digitized on an Eikonix IEEE-488 camera with a square-pixel size corresponding to 5.3 (×45,000 negatives) or 6 (×40,000 negatives) Å/pixel. General image processing operations were carried out using the PIC Software system (76) running on an Alpha workstation DPW600au (Compaq). Particles were extracted and preprocessed using the automated procedure of Conway et al. (14). Particle orientations were determined by "common-lines" procedures of Fourier analysis (4, 15, 25). Model-based procedures were used for all subsequent orientation and phase origin refinements (3). For reconstruction of the small VP2 capsid, only model-based procedures were used, and as a starting model we used another small VP2 capsid extracted from the large VP2 capsid. As an internal control, the three-dimensional structure of large VP2 particles was calculated without imposing icosahedral symmetry by using a weighted-backprojection method and distributing the orientations over the whole orientation space by randomly selecting equivalent views that were related by symmetry to the originals (67, 76). The resulting density map, calculated from 412 particles and without any refinement steps, was visually similar to that obtained with the icosahedral symmetry-based method (data not shown).

Reconstructions, with a set of particles that adequately represented the icosahedral asymmetric unit, were calculated using Fourier-Bessel techniques (15), and complete icosahedral (532) symmetry was imposed in the final density maps. The underfocus value of the selected electron micrographs permitted reconstructions of the structures to a resolution within the first zero of the CTF of the electron microscope. No corrections due to CTF were incorporated in the reconstruction.

Each reconstruction was based on data from several micrographs taken in the same session to include in the final model 72 images of "large VP2 particles," 33 images of "small VP2 particles," and 75 images of IBDV particles. The number of particles in each set was initially larger, but many particles had to be excluded because their orientations could not be determined, presumably because they were either incomplete or broken. The resolution of the final reconstructions was estimated to be ~28 Å in terms of the spatial frequency at which the Fourier ring correlation coefficient dropped below a resolution-dependent value expected for random models (threshold of statistical significance) (14, 71). Data quality was also assessed by eigenvalue spectra (26). At the resolutions achieved, 99 to 93% of the mean inverse eigenvalues of the 72, 33, and 75 particles were less than 0.01, indicating that the data were adequately sampled in the Fourier space (16). The reliability of the reconstructions was also tested by reprojecting the three-dimensional maps along the orientations of the individual particles included in the reconstructions.

RESULTS

Expression and characterization of IBDV VPX and VP2 proteins. The baculovirus AcVPX.IBDV contains a 1,548-nucleotide insert, which expressed a 516-amino-acid protein. The baculovirus AcVP2.IBDV contains a 1,368-nucleotide insert, which expressed a 456-amino-acid protein. VPX and VP2 proteins were expressed in insect cells and purified by a sucrose cushion followed by a sucrose gradient. Fractions containing VPX banded in a broad rage of densities (1.142 to 2.212 g/cm^3), while VP2 banded at a density of 1.091 g/cm^3. VPX and VP2 were concentrated and characterized by SDS-PAGE, Western blot analysis, and electron microscopy (Fig. 1A). Coomassie blue staining of SDS-PAGE gels showed that the fractions enriched in VPX and VP2 were very pure. VPX consisted of a doublet of peptides of ~48 kDa, while VP2 consisted of a single polypeptide of ~41 kDa (Fig. 1B). The doublet of VPX may represent different cleavages of the protein (70) or, as has been demonstrated for bacteriophage ϕ6 (17), a variable unfolding which alters its migration. The VPX/VP2-monospecific serum specifically recognized both proteins (Fig. 1C). As a control, a sample of purified IBDV particles was also analyzed (Fig. 1B and C).

Analysis by electron microscopy of these fractions, enriched, respectively, in VPX or VP2, revealed two different morphologies. VPX led to the formation of twisted tubular structures, 16 to 30 nm in diameter, which probably reflect different flattening degrees (Fig. 2A). Although these tubular structures were presumably built up by only one structural block of VPX, they were too poorly ordered to be analyzed by Fourier methods. However, their powder patterns revealed spots in the first order following a hexagonal lattice; this allowed us to determine the unit cell dimensions of VPX tubes, which are ~10 nm, extending in some cases to 13 nm. VP2 seems to form a doughnut-shaped structure, ~23 nm in diameter. All VP2 particles showed a centered cavity filled with the negative stain agent (Fig. 2B). IBDV samples were also analyzed, and the typical polygonal contour, with a diameter of 65 to 70 nm, was observed (Fig. 2C).

Cryoelectron microscopy of VP2 particles and IBDV. The major advantage of cryoelectron microscopy over conventional electron microscopy techniques is that biological macromolecules are observed in a frozen hydrated state in amorphous ice

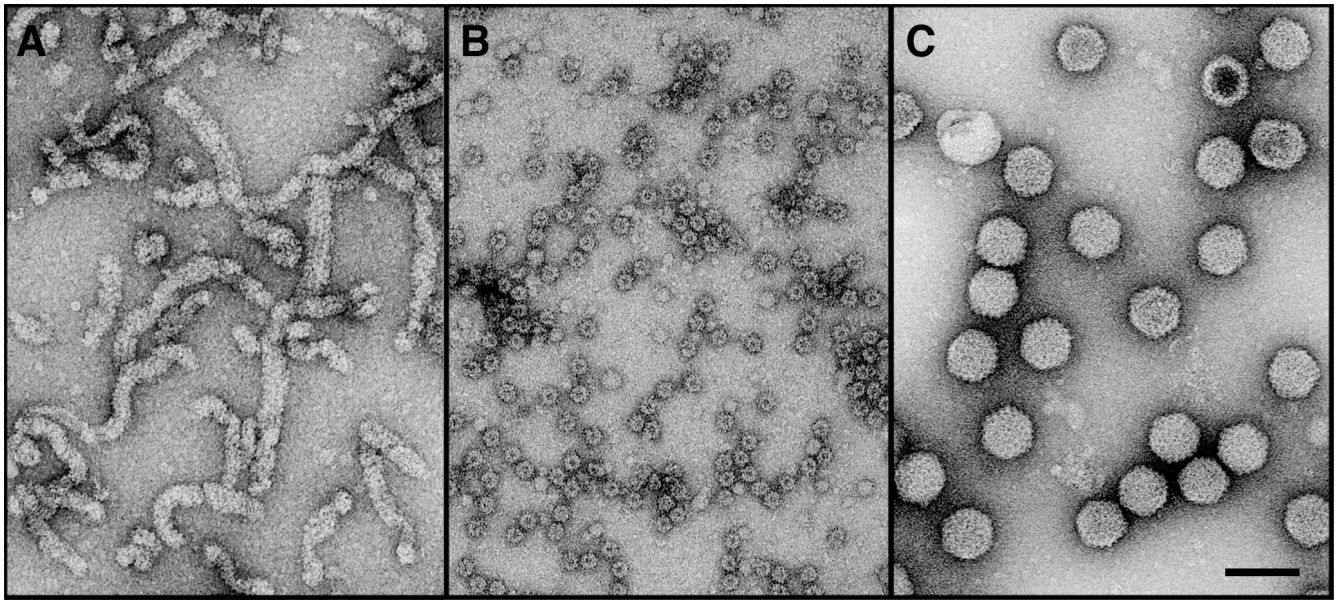

FIG. 2. Electron microscopy of VPX and VP2 assemblies, compared with IBDV virions. (A) VPX twisted tubular structures; (B) VP2 doughnut-like structures; (C) purified IBDV virions. Bar, 100 nm.

that closely resembles the native aqueous state. For that reason VP2 structures were analyzed by cryoelectron microscopy. The doughnut-shaped structures were also observed by this technique, but in a smaller proportion than other, larger structures, 55 to 65 nm in diameter (Fig. 3A). These bigger structures, which will be referred to as "large VP2 capsids," are most likely formed from the doughnut-like structures, referred to as "small VP2 capsids," since no proteins other than VP2 were

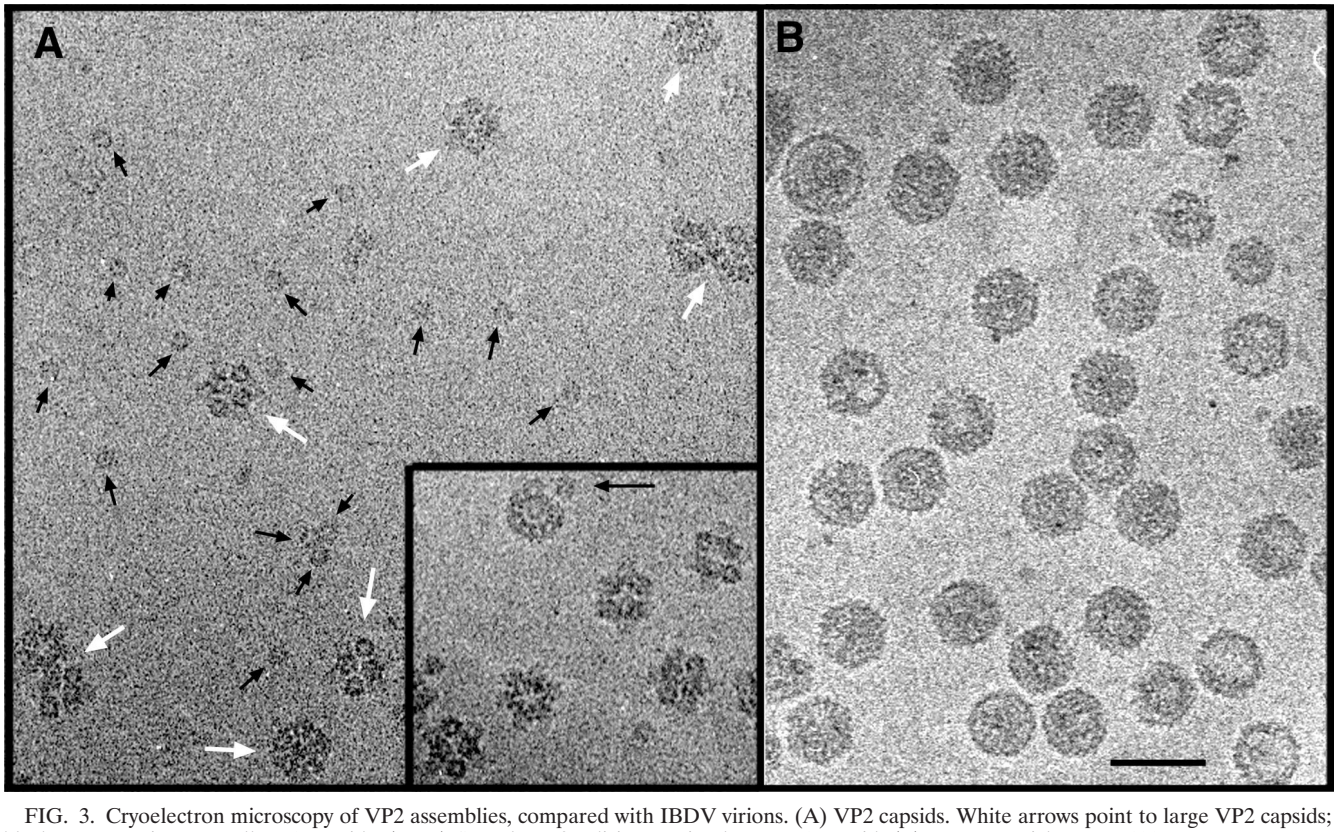

FIG. 3. Cryoelectron microscopy of VP2 assemblies, compared with IBDV virions. (A) VP2 capsids. White arrows point to large VP2 capsids; black arrows point to small VP2 capsids. (Inset) Snapshot of a disintegrating large VP2 capsid. (B) IBDV particles. Bar, 100 nm.

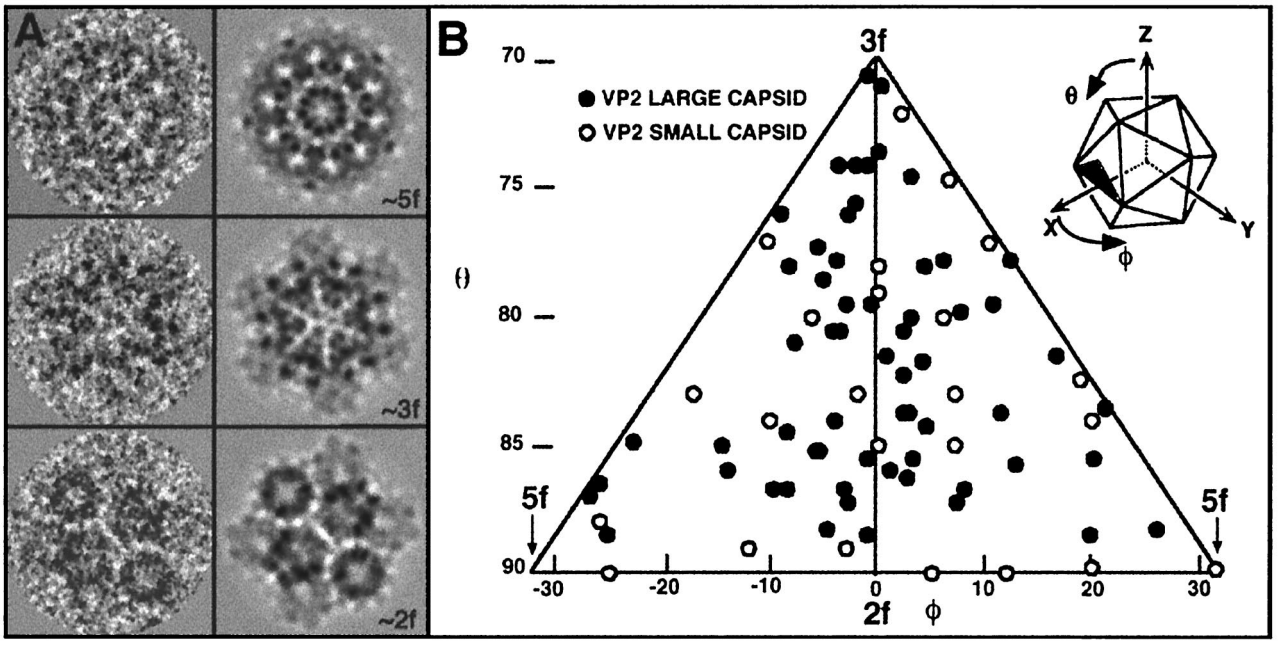

FIG. 4. Evaluation of the icosahedral symmetry of large VP2 capsids and orientations of small and large VP2 particles. (A) Images of large VP2 capsids taken directly from the original cryomicrograph (left column), compared to the projected view (right column) of the three-dimensional reconstruction in the corresponding orientation. Selected large VP2 capsids oriented close to a fivefold (~5f) (top), threefold (~3f) (center), or twofold (~2f) (bottom) axis of symmetry are shown. (B) Plot of the refined orientations determined for particles used to compute the three-dimensional maps. The orientation of each particle is mapped in the icosahedral asymmetric unit (shaded region in the icosahedron in the upper right corner). θ and φ are the angles that specify the orientation of the capsid relative to the view direction. The icosahedral fivefold (θ = 90.0°, φ = ±31.72°), threefold (θ = 69.09°, φ = 0.0°), and twofold (θ = 90.0°, φ = 0.0°) axes are indicated.

present in the fractions analyzed (Fig. 1B and C). In some cases, we were able to take snapshots of disintegrating large VP2 capsids lacking one of these smaller constitutive elements (Fig. 3A, inset).

For comparison, IBDV capsids were also analyzed by cryoelectron microscopy. They were, as described, ~70 nm in diameter at their widest points (Fig. 3B). They showed a polygonal rather than circular contour, and distinct serrations were visible around their peripheries. Dark areas inside the capsid may reflect different degrees of dsRNA packaging.

Structure of large VP2 capsids. Images from electron cryomicrographs of large VP2 particles revealed a peculiar arrangement of structural units following icosahedral symmetry. The fivefold, threefold, and twofold views were relatively abundant and clearly observed (Fig. 4A, left column). The three-dimensional structure of large VP2 capsids was determined by using 72 particles whose orientations were distributed fairly uniformly in the icosahedral asymmetric unit (Fig. 4B). To confirm that the orientation of each particle had been correctly determined, the three-dimensional map was reprojected in the appropriate viewing geometry and compared with the original images both visually (some examples are shown in Fig. 4A; compare left and right columns), and by quantitative criteria (the Fourier ring correlation method) (Fig. 5).

Surface representations of the three-dimensional reconstruction of a large VP2 capsid along the icosahedral five-, three-, and twofold axes are shown in Fig. 6A. This model shows 532 symmetry, but it was obtained by a reconstruction procedure imposing only 522 symmetry. The map was contoured in such a way that a continuity of density is observed, although some putative small holes may appear filled (see below). The capsid size ranges from ~60 to ~68 nm in diameter. This structure is an icosahedron built up by 12 smaller dodecahedra, one in each vertex of the icosahedron, leaving an

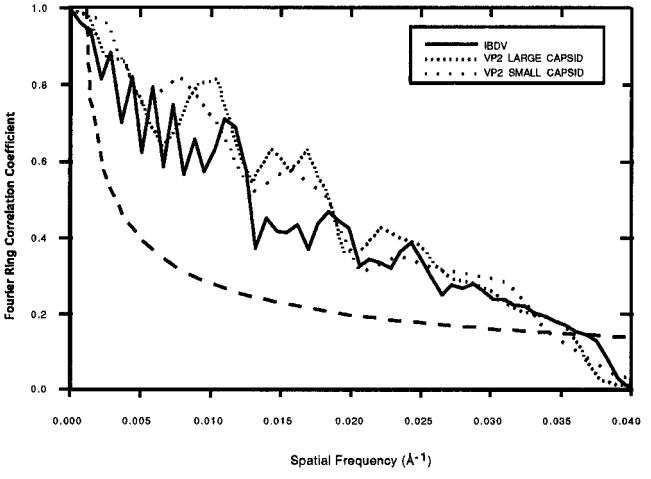

FIG. 5. Resolution assessment by Fourier ring correlation function for three-dimensional reconstructions of large VP2, small VP2, and IBDV capsids. The resolution limits determined from these plots are ~29 Å (a spatial frequency of ~0.034 $Å^{-1}$) for the small VP2 capsid and ~28 Å (a spatial frequency of ~0.036 $Å^{-1}$) for the large VP2 and IBDV capsids. The dashed line represents an estimate of the significance level of resolution (this is $2/\sqrt{n}$, where n is the number of samples at a particular spatial frequency).

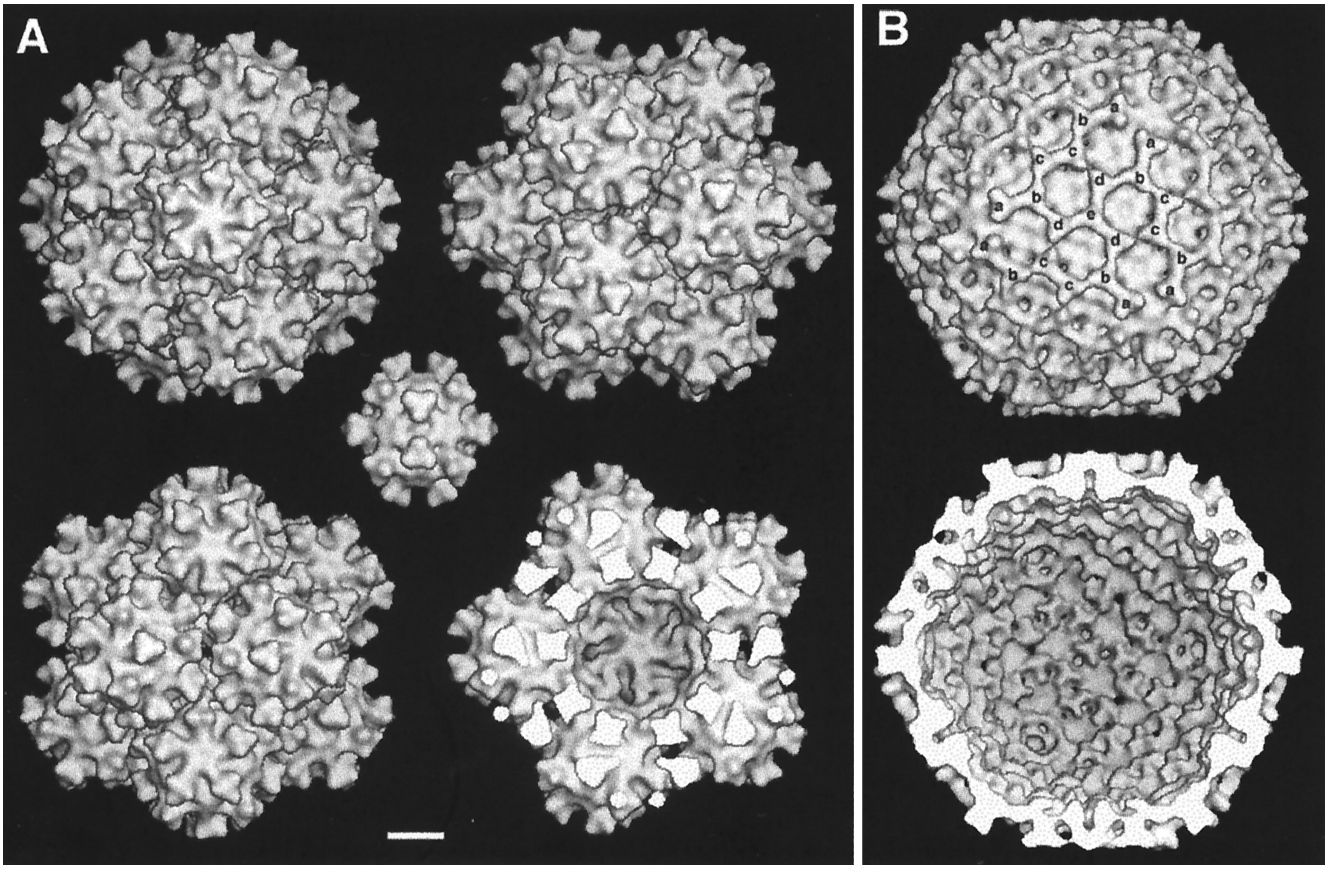

FIG. 6. Three-dimensional structure of the large VP2 capsid and the IBDV capsid. (A) Surface-shaded representations of the outer surfaces of large VP2 capsids viewed along a fivefold (top left), a threefold (top right) and a twofold (bottom left) axis of icosahedral symmetry. A model with the front half of the protein shell removed, viewed along a fivefold axis, is shown at the bottom right. For size comparison, a three-dimensional map of a small VP2 capsid, viewed along a twofold axis, is shown in the center. (B) Surface-shaded representations of the outer (top) and inner (bottom) surfaces of IBDV capsids viewed along a threefold axis of icosahedral symmetry. The five different types of trimeric capsomers are indicated by the letters a to e. Bar, 100 Å.

almost-closed internal cavity in the middle, as shown in the view down the icosahedral fivefold axis with the front half of the capsid removed (Fig. 6A, bottom right). The internal cavity is formed by the contribution of one pentagonal face of each dodecahedron. The T=1 dodecahedron is characterized by 20 protruding structures at the vertices, and because of them, the internal cavity of the large VP2 capsid is not occupied. The protruding units, as expected, show a trimeric profile, with each trimeric unit contributing to three pentagonal faces. Therefore, T=1 capsids would be made up of 60 VP2 subunits, and the large VP2 particles would have 720 subunits. The five trimeric protrusions of each dodecahedron oriented toward the inner cavity interact with another two. It appears that the inside of the dodecahedral capsid, as well as the internal cavity, is empty. A more detailed analysis of the T=1 capsid is given below.

Structure of IBDV capsids. For purposes of comparison, a three-dimensional reconstruction of IBDV particles was also calculated (Fig. 6B). The IBDV capsid shows the same structural features as those described by Böttcher et al. (8), although the resolution was limited to 28 Å in our map (Fig. 5). The surface-shaded maps were contoured to enclose a volume showing the same features as those previously published by Böttcher et al. (8). The capsid is icosahedral and exhibits a T=13 lattice, shown in the right-handed form as shown by Böttcher et al. (8), where 260 units protruding from a continuous shell are trimer clustered. Even at this moderate resolution, five different classes of triangular capsomers can be distinguished depending on their different local environments (labeled "a" to "e" in Fig. 6B). At the present resolution, as in previous work, significant changes can be observed between the various quasi-equivalent trimers. This fact is reflected in the interactions of each trimer with their neighbors. Class e trimers, located at the strict icosahedral threefold axis, interact rather closely with their neighbors, showing three thick arms connecting with surrounding trimers of class d. Class c and d trimers, which are enantiomorphs, show two connecting arms, one thick and another thinner. Trimers of class b also show three connecting arms, only one of which is thick. And trimers of class a, located around the strict icosahedral fivefold axis, have one thick arm connecting with trimers of class b. Following the "mnemonic rule" initially formulated for bluetongue virus (BTV), trimer a in IBDV corresponds to trimer P in BTV, b corresponds to Q, c to S, d to R, and e to T. These connecting arms form an arch-like structure located from a radius of ~31 nm out to ~35 nm. Under these arches, there

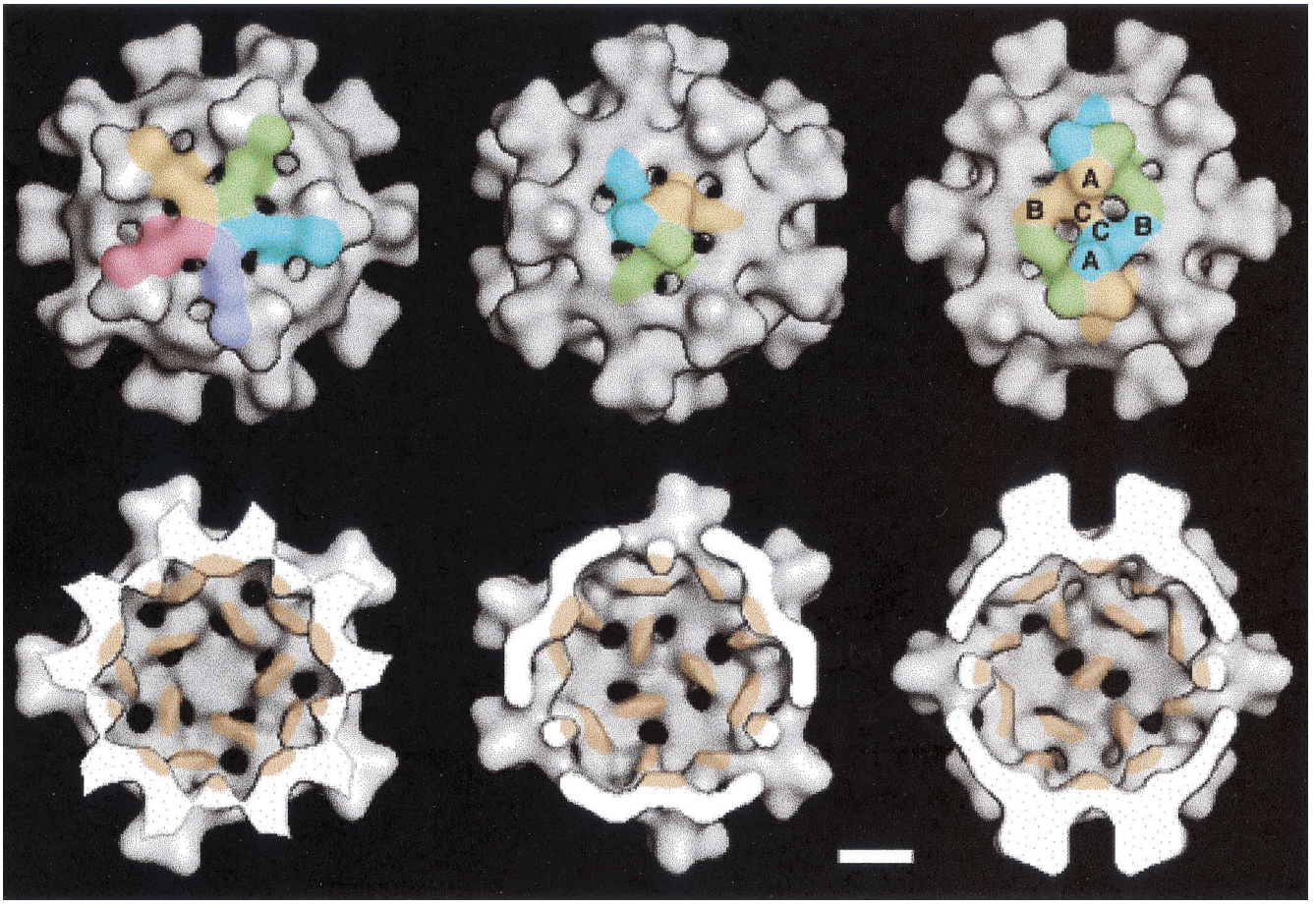

FIG. 7. Three-dimensional structure of the small VP2 capsid. Shown are surface-shaded representations of the outer (top row) and inner (bottom row) surfaces of small VP2 capsids viewed along a fivefold (left column), a threefold (middle column), and a twofold (right column) axis of icosahedral symmetry. T=1 pentamers are shown with the same handedness as T=13 pentamers. Different VP2 subunits are indicated by different colors. In the twofold view, two subunits are subdivided into the three proposed domains (A, B, and C). The internal protrusions, located at the icosahedral twofold axis, are tinged with orange (bottom row). Bar, 50 Å.

appear to be small pores in the thin continuous shell, six around the local sixfold axis, except in those around the pentamers, where there appear to be five pores. The only gaps of density observed between adjacent trimers are between c and d trimers and between a and a trimers. On the inner shell, there are only 200 trimeric structures (Y-shaped structures). The five expected trimers surrounding each pentamer are replaced by a density which forms an annular rim around another concentric rim. This smaller rim almost closes a pentagonal cavity at the fivefold position. It should be noted that the previously published CTF-corrected IBDV structure (8) does not show this small rim of density. Whereas the vertices of inner trimers point to the center of the hexamers (local sixfold axis), the outer trimers are rotated ~60°, with their triangular edges facing the local sixfold and fivefold axes. The outer trimers extend outward by ~4 nm from the thin shell, ~2 nm thick, whereas the inner trimers extend inward by ~3 nm.

Structure of small VP2 capsid. One dodecahedron was extracted from the large VP2 capsid reconstruction and used as an initial model to find orientations of the small VP2 capsids, probably produced after disassembly of the larger capsids (Fig. 3A). The three-dimensional reconstruction of small VP2 particles, at a resolution of 29 Å (Fig. 5), showed the same arrangement as the empty T=1 dodecahedron that forms part of large VP2 particles (Fig. 7). Surface-shaded representations of small VP2 capsid were based on the assumption that 60 VP2 molecules make up each capsid and on taking a value of 0.73 cm^3/g as the partial specific volume of protein. At this threshold level, the capsid was perforated by five small holes, ~1.5 nm in diameter, around each fivefold position. Trimeric protrusions were conformationally equivalent, since they had the same local environment. In comparison with the outer trimeric units of the IBDV capsid, they did not show any arms connecting to each other, although the size and general topography were essentially identical. The capsid wall was formed by connected densities that were arranged at two different radii: 12 pentagonal platforms around the fivefold axis at an average radius of ~9 nm and 20 smaller islands of density at an average radius of ~7 nm, extending further inward at the twofold axis (Fig. 7, bottom). On the outer surface, the trimeric units protruded ~3.5 nm from the pentagonal platform. Thus, the general shape of each monomer of VP2 may be envisioned (Fig. 7, top). Due to the handedness shown by these T=1 capsids, we have assumed the right-handed form as with virion particles.

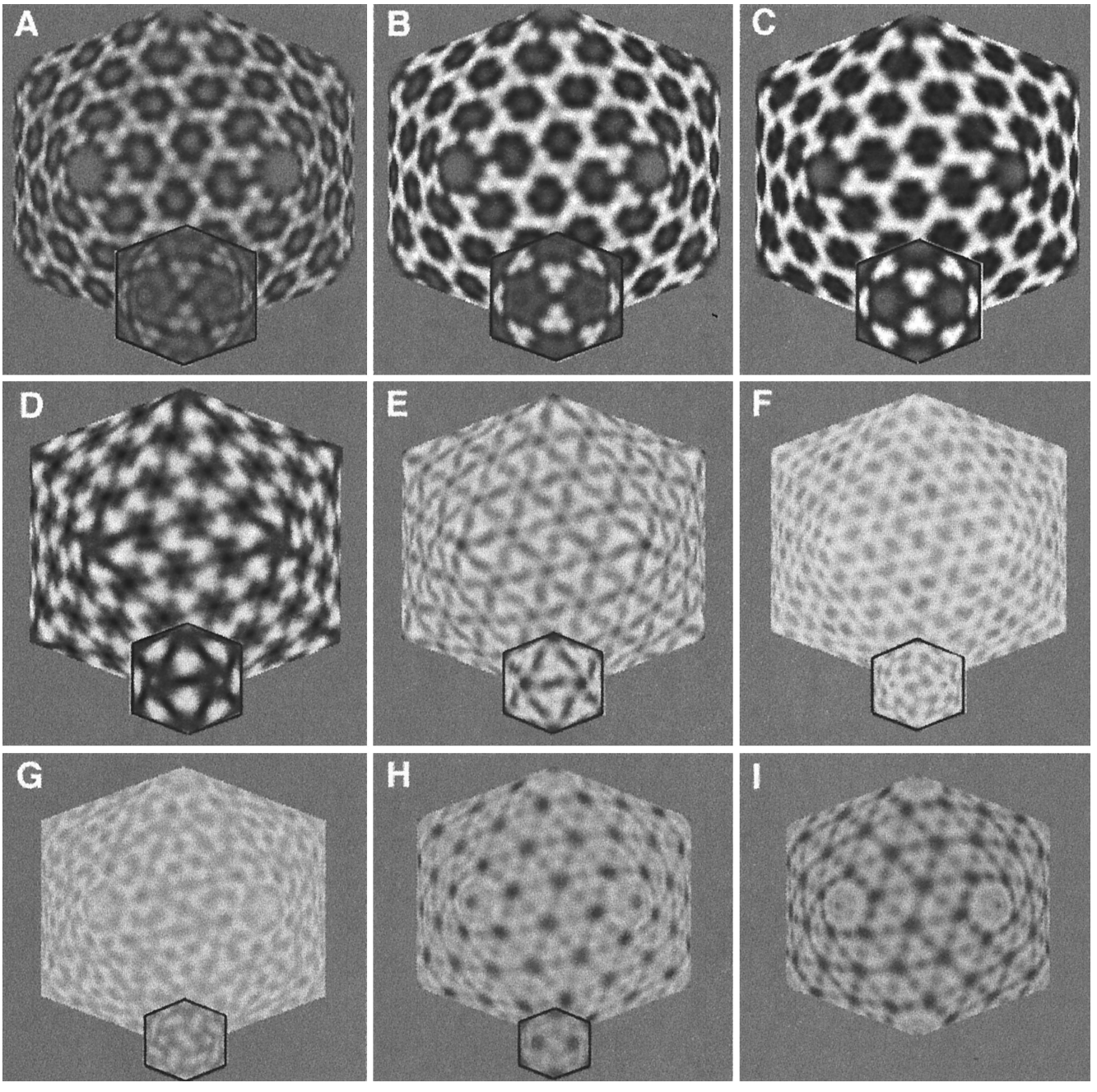

FIG. 8. Structural organization of IBDV and small VP2 capsids. Shown are icosahedral sections of scaled three-dimensional maps of the IBDV capsid (large hexagon in each panel) and the small VP2 capsid (smaller hexagon at the bottom center of each panel), viewed along a twofold axis. The range of sections shown is from 34 (A) to 26 (I) nm for the IBDV capsid and from 13.5 (A) to 6.5 (H) nm for the small VP2 capsid, with a radial step of 1 nm between sections. The IBDV capsid extends to a 24-nm radius (not shown). The perpendicular distances of the faceted icosahedral sections from the center of the IBDV capsid are 34 (A), 33 (B), 32 (C), 31 (D), 30 (E), 29 (F), 28 (G), 27 (H), and 26 nm (I); from the center of the small VP2 capsid, these distances are 13.5 (A), 12.5 (B), 11.5 (C), 10.5 (D), 9.5 (E), 8.5 (F), 5.5 (G), and 6.5 (H) nm.

Comparison of small VP2 and IBDV capsids. The apparent similarity of outer protruding trimers of small VP2 and IBDV capsids made feasible the comparison of carefully scaled structures of the three-dimensional maps of IBDV and small VP2 capsids. Since both capsids were quite far from the spherical shape, they were sampled on icosahedral sections in order to conveniently compare equivalent features by using the "facets" program (kindly provided by R. A. Crowther [8]).

Maps were aligned in such a way that the protruding outer trimers start at the same outermost icosahedral section (Fig. 8). The outermost sections (~31 to 34 nm and 13.5 to 10.5 nm for IBDV and small VP2 capsids, respectively) show that the external trimeric units have the same size and morphology at this resolution (Fig. 8A through D). Further in (30 and 9.5 nm, respectively), the trimers adopt an extended triangular profile, but with the vertices pointing toward the centers of pentamers

and hexamers, constituting a ring of density (Fig. 8E). At a 29-nm radius (and at an 8.5-nm radius), these rings become more evident (Fig. 8F) and form the beginning of the continuous shell in the IBDV capsid (Fig. 8G). At a 28-nm radius (and at a 7.5-nm radius), the densities of the IBDV and small VP2 capsids are not directly comparable; whereas in the IBDV capsid the shell is still continuous, in the small VP2 capsid there are only remainders of densities at the strict twofold axis, which clearly ends at a 27-nm radius (Fig. 8H). On the sections corresponding to the inner surface of the IBDV capsid (27 to 26 nm) the Y-shaped features are visible, except around the fivefold axis, where two concentric rings of density surrounding each fivefold position are present (Fig. 8H and I).

Due to the fact that small VP2 capsids are exclusively made up of VP2, they offer the possibility to define the likely boundaries of the monomer of this protein. Each VP2 molecule can be considered to be subdivided into three domains, called A, B, and C (see Fig. 7, top right, and schematic diagram in Fig. 9, top left). From the outer surface, each VP2 molecule is a cylinder-like domain (called domain A), ~2.5 nm in diameter and ~4 nm long (sections from 13.5 to 10.5 nm [Fig. 8A through D]), that interacts extensively with another two A domains, constituting the protruding trimeric unit. At this height (~4 nm from the top), an arm of density, ~1 nm in diameter (called domain B), emanates from each A domain toward three different fivefold positions (sections from 9.5 to 8.5 nm [Fig. 8E and F]). Further in (sections from 7.5 to 6.5 nm [Fig. 8G and H]), the cylinder-shaped structure becomes curved (designated domain C), is directed to the twofold axis, and meets with another domain C from a VP2 molecule of an adjacent trimeric unit. The overall length of the trimer is ~70 Å along the local threefold axis, formed by domains A and C.

The VP2 polypeptides are interconnected through different kinds of interactions that consolidate the capsid structure. Intratrimeric interactions occur extensively through A domains at the threefold axis stabilizing the VP2 trimers, whereas intertrimeric interactions effected by B-B interactions occur around the fivefold axis and those effected by C-C interactions occur deeper in the lattice at the twofold axis (see Fig. 7, top right). One interesting feature of the capsid structure is that B-B interactions stabilize the pentamers; however, interpentameric interactions take place at the threefold axis via A-A interactions and, to a lesser extent, at the twofold axis via C-C interactions. Considering the most compact arrangement, the basic protomer should be a VP2 trimer, since the pairing in which subunits interact across the twofold axis involves a smaller contact surface.

DISCUSSION

General features of dsRNA viruses. Although dsRNA viruses are a rather diverse group, they share general architectural principles and numerous functional features (41). They have segmented genomes, and two or three concentric icosahedral shells usually form virion capsids (5). Whereas the outer layer is involved in protection, adhesion, and cell entry, the innermost layers are specialized compartments for transcription and replication of the dsRNA genome. A T=13 icosahedral shell composed of 260 trimeric clusters (or 200 trimers in incomplete T=13 shells) seems to be a common feature of dsRNA viruses. It is observed in BTV of the genus *Orbivirus* (32, 66), orthoreovirus (20, 55), rotavirus (65, 79), phytoreovirus (e.g., rice dwarf virus) (50), aquareovirus (62, 72), and bacteriophage φ6, a member of the *Cystoviridae* family (10, 17). The other ubiquitous capsid structure observed is a "T=2" lattice, present in all viruses described above, as well as in dsRNA fungal viruses, such as L-A and P4 (12, 13), and insect cypoviruses such as cytoplasmic polyhedrosis virus (33, 80) (Table 1). L-A virus lacks an outer T=13 layer because its life cycle is entirely intracytoplasmic (78), and cytoplasmic polyhedrosis viruses are embedded within large crystalline inclusion bodies, proteinaceous polyhedra which act as transmission vehicles. IBDV is unique among dsRNA viruses in having a single capsid based on a T=13 layer and in lacking the supposed general replicative machine based on a T=2 layer, at least in the mature virions. Neither our studies nor previous structural analysis (8) has shown the presence of a T=2 layer. Biochemical and genetic analyses of infectious viral particles demonstrate that there is no protein candidate that could form a structure with 120 molecules arranged in a T=2 capsid, as observed in other dsRNA viruses (see, e.g., references 12, 30, 42, 56, and 68). However, we cannot discard the possibility that some of the major structural proteins are able to assemble into a 120-subunit capsid, as was shown with the capsid protein of brome mosaic virus, a plant virus which normally assembles into T=3 capsids (40).

Molecular anatomy of the IBDV capsid. The general architecture of IBDV strain Soroa, analyzed here, is essentially identical to that of the strain isolated from Russia. Our studies extend the analysis of the supramolecular organization of IBDV particles from that of Böttcher et al. (8), because we have included a comparison between IBDV capsids and small VP2 capsids, which are formed only by the VP2 major structural protein. These new results provide conclusive information on the specific structural features of most of the viral proteins and on the quaternary organization of the major structural proteins, VP2 and VP3. Figure 9 is a schematic diagram showing the supramolecular organization of the T=13 layer of IBDV. 9. All details in this discussion are represented in that model.

From comparative analysis between the IBDV capsid and the small VP2 capsid, we conclude that VP2 subunits, constituting ~51% of the protein in infectious virions (18), are displayed in the virion structure as 260 trimeric clusters of outer protruding structures. This VP2 location is not only in good agreement with a previous hypothesis based on stoichiometry and structural analysis (8) but also justifies the fact that VP2 carries the dominant neutralizing epitopes (23). Since VP3 is expected to interact with the RNA genome (35) and the whole molecule is inaccessible to specific antibodies (51), it is clear that VP3 is on the inner surface of the capsid. Therefore, it is reasonable to assume that the 200 Y-shaped trimeric structures located at the inner surface of the shell correspond to VP3 (~40% of the protein in infectious virions). Considering that VP3 also interacts in vivo with VP1, the viral RNA polymerase (48, 75), the proposed location of VP3 is consistent with its function as an intermediary between VP1 and VP2. Obviously, taking into account the small amount of VP1 in mature virions (~3% of the protein), only a minor population of VP3 molecules would interact with VP1.

TABLE 1. Structural elements of dsRNA virus capsids[a]

Virus family	Multilayered capsid features[b]										No. of dsRNAs
	Outermost layer			Intermediate layer			Innermost layer				
	T[c]	ϕ (Å)[d]	Protein(s)[e] (mol wt)	T	ϕ (Å)	Protein(s)[e] (mol wt)	T	ϕ (Å)	Protein(s)[f] (mol wt)	Turret[g]	
Reoviridae											
Orthoreovirus	$13l_i$	~850	**σ3** (41), σ1 (51)	$13l_i$	~800	**μ1** (76)[h]	2	~600	σ2 (47)[i] **λ1** (142), λ2 (144)	+	10
Rotavirus	13l	~765	**VP7** (37), VP4 (87)	13l	~705	**VP6** (41)[j]	2	~520	**VP2** (94)	−	11
Orbivirus	NA	~900	VP2 (111), VP5 (59)	13l	~690	**VP7** (37)	2	~520	**VP3** (103)	−	10
Aquareovirus	$13l_i$	~820	**VP7** (35), VP5 (71), VP4 (73)	NP	NP	NP	2	~600	**VP3** (126), **VP6** (46)[k] VP1 (130)	+	11
Phytoreovirus	13l	~700	**P8** (46)	NP	NP	NP	2	~570	**P3** (114)	−	12
Cypovirus	NP	NP	NP	NP	NP	NP	2	~580	ND	+	10
Cystoviridae, phage ϕ6	13_i	~580	**P8** (16)[l]	NP	NP	NP	2	~500	**P1** (85), P2 (75), P4 (35)	+	3
Totiviridae, L-A, P4	NP	NP	NP	NP	NP	NP	2	~430	**Gag** (76)	−	1
Birnaviridae, IBDV	13	~700	**VP2** (41), VP3 (32)	NP	NP	NP	NP	NP	NP	−	2

[a] Data are taken from references 8, 10, 12, 13, 17, 20, 30–33, 42, 50, 55, 62, 64–66, 68, 72, 78, 79, and 80.
[b] NA, not applicable; NP, not present; ND, not determined.
[c] T, triangulation number; T=$13l_i$, incomplete T=13l shell.
[d] ϕ, outer diameter.
[e] Only major proteins are indicated; T=13 shell-forming proteins are indicated in bold.
[f] Only major structural proteins are indicated; T=2 shell-forming proteins (120 monomers) are indicated in bold; proteins making turret-like structures are underlined; transcriptional complex proteins are omitted.
[g] +, present; −, absent.
[h] Reovirions lacking the outermost layer are known as intermediate subviral particles (ISVPs).
[i] σ2 protein is present in a copy number of 150 on the T=2 core.
[j] Intermediate and innermost layers of rotavirus are known as DLPs (double-layered particles).
[k] There are 2 major proteins in a copy number of 120 subunits in aquareovirus.
[l] The outermost layer of phage ϕ6, called nucleocapsid (NC), is surrounded by a lipid bilayer and a lysozyme layer.

Plots of spherically averaged density as a function of radius for the computed map of the IBDV particles show a unique peak of density (data not shown), indicating that both proteins in close proximity form the continuous shell surrounding the internal mass (genome and minor proteins). The close VP2–VP3 interaction can be visualized at a 28-nm radius (Fig. 8G).

The best structurally characterized proteins forming a T=13 icosahedral shell in dsRNA viruses are VP7 (37 kDa) of BTV and VP6 (41 kDa) of rotavirus, which have an outer domain with a typical β-sandwich fold and an inner domain consisting of a bundle of α-helices (29, 31, 53). The shape of VP2 (41 kDa) suggests a three-domain structure, since we have considered the inner domain as subdivided into halves. Nevertheless, the outer morphologies of BTV VP7 (or rotavirus VP6) and VP2 of the small VP2 capsid are quite similar.

The largest differences between BTV VP7 and VP2 trimers are found at the lower domain. BTV VP7 trimers are arranged around a fivefold axis and a local sixfold axis, leaving prominent holes at the centers of pentamers and hexamers (31, 66), in a manner similar to that of rotavirus VP6 (53, 64). However, VP2 closes those holes with the B domain, and probably some regions of VP3 also contribute to the platforms at the local sixfold axis. Besides, BTV VP7 trimers are anchored on the surface of a T=2 core, made by BTV VP3, by relatively nonspecific interactions (30). The assembly scenario for IBDV VP2 trimers is completely different; their bases are in close contact with trimers of VP3 that do not form an internal continuous network (the T=2 innermost core structure).

Large VP2 capsids. Overexpression of VP2 leads to production of large structures built up by 12 dodecahedra arranged in a quasi-icosahedral supercapsid. This unique arrangement probably reflects a natural tendency of VP2 trimers to interact, a feature that can eventually lead to the crystalline arrangements of viral particles found inside IBDV-infected cells. As far as we know, there are no other examples of high-order assembly of VLPs following this geometry, and studies of their possible uses for vaccination or content delivery are under way.

Tubular structures of VPX and functional implications. Notably, many structural proteins of dsRNA viruses that assemble as 260 trimers with a complete T=13l (*levo*) icosahedral lattice also form planar and tubular hexagonal arrangements: VP7 of African horsesickness virus, which is structurally similar to BTV VP7 (9); P8 of the phytoreovirus rice dwarf virus (81); and VP6, the protein making the T=13l lattice of double-layer particles of rotavirus (34, 46, 63). VPX/VP2 also has a natural propensity to form highly ordered hexagonal tubes (51).

VPX protein, when expressed alone, assembles into twisted tubular structures with a "weak" hexagonal symmetry. When expressed from the complete polyprotein in various baculovirus-based systems, it assembles forming highly ordered hexagonal tubes, or as intermediate tubular structures, called capped flexible tubules (51). Despite the slight differences in morphology, rigid, flexible, and twisted tubules of VPX correlate well, showing a unit cell with similar dimensions. Interestingly, VPX rigid tubules colocalized with VP3 in transformed cells, forming a conspicuous network, but VP3 is lost during purification.

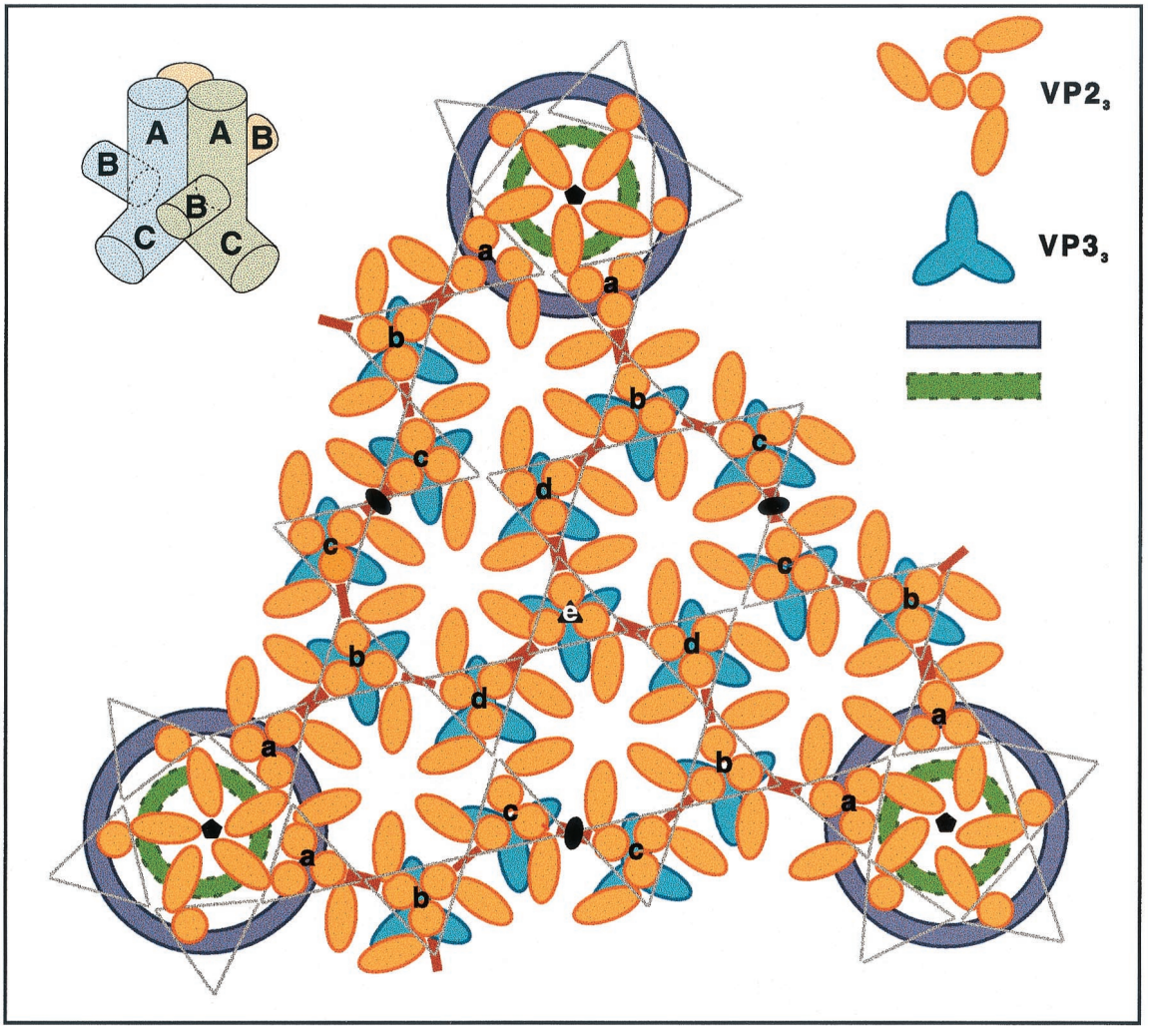

FIG. 9. Schematic diagram showing subunit interactions in the T=13 layer of IBDV. A complete icosahedral face is shown. VP2 trimers (orange) are superimposed on VP3 trimers (blue), and a simplified version of their shapes is given for clarity. The five classes of trimeric VP2 units are represented by letters a to e. Thin and thick connecting arms between VP2 trimers, as observed on the surfaces of IBDV capsids, are shown in red. Annuli around the fivefold positions (green and violet) are unassigned features (see Discussion for details). Two-, three-, and fivefold axes are indicated by conventional symbols. (Top left) Schematic diagram showing arrangement of VP2 subunits in the trimeric protrusions of the T=1 surface lattice.

The VP3 content of flexible tubules is restricted to the caps of the tubes. Two-dimensional comparisons showed that VPX trimeric tubular capsomers from rigid and flexible tubules are almost identical to IBDV VP2 trimeric clusters (8, 51). These findings, taken together with our results, suggest that VP3 plays a stabilizing role in the connections between equivalent VPX trimers of identical hexamers, at least temporally, since if VP3 is absent, the order in the tubular structure is low, leading to twisted tubules. Interhexameric connections in the IBDV capsid take place at the threefold axis via A domains, and VP3 is found beneath the base of the VP2 trimers. These two facts reinforce the hypothesis about the stabilizing function of VP3.

Molecular switching mechanism. Each virus displays a switching mechanism for altering subunit interfaces and/or conformations required for the assembly of quasi-equivalent capsids (36). The major differences between IBDV VP2 trimers are clearly reflected at the top domain, where arch-like structures of variable thickness are observed, regardless of the contour display level. These differences are observed in our 28-Å resolution map as well as in the CTF-corrected IBDV structure published previously (8). Interestingly, these upper connections are not observed in any other T=13 capsid of dsRNA viruses, probably indicating that the quasi-equivalence principle is loosely followed by the IBDV capsid. Therefore, VP2 must undergo significant conformational changes upon adopting the quasi-equivalent locations on the T=13 lattice, illustrating a remarkable level of nonequivalence. This is probably the reason why VP2 trimeric capsomers in the IBDV capsid are not as well defined as in the VP2 capsids. Domains B and C, forming the base of VP2 trimers, must also undergo specific conformational changes. Thus, for example, VP3 is not found, at least as a trimeric structure, in the base of pentameric VP2 trimers.

From our results, we can infer that the VPX C-terminal tail,

a region that comprises 50 to 60 residues, is crucially involved in the control of the interactions between VP2 trimers and between VP2 trimers and VP3 trimers. When this C-terminal region is completely removed, VP2 assembles in vivo into a dodecahedral structure where all trimers have identical interactions. Since assembly of these T=1 capsids proceeds independently of any other IBDV proteins, the information to form the T=1 closed surface must be intrinsic to the subunits themselves. Thus, VP2 can form only T=1 capsids, probably because elimination of the C-terminal region has abolished the expected inherent flexibility, as no other aberrant shell-related structures are formed. This observation suggests that the C terminus of VPX may provide more-flexible subunit contacts. However, the possibility that VP3 may also be involved as an alternative or complementary switching mechanism cannot be ruled out. An argument against this role of VP3 is the fact that when VP2 is coexpressed with VP3, small VP2 capsids with a morphology similar to that obtained with VP2 alone are observed by negative staining (data not shown). A switching mechanism has been described in an unrelated system, yeast Ty retrotransposons, which assemble into VLPs with different T numbers depending on the C-terminal length of the capsid protein (1).

Control of assembly pathway. The in vivo assembly pathway of IBDV has not been rigorously determined. The strong structural similarities between pentamers of the virion and small VP2 capsids suggest that their assembly may share intermediates. Both capsids may initiate assembly with trimers of VP2 that would form pentamers upon nucleation of additional equivalent (T=1 capsids) or nonequivalent (T=13 capsids) trimers. The formation of pentamers, as well as interpentameric interactions, is independent of the presence of VP3. In contrast, interhexameric interactions give rise to more-labile structures and require VP3 to maintain their integrity (see above).

Most VPX is found as VP2 in the mature virion, as deduced from their patterns in SDS-PAGE analysis. Site-directed mutagenesis analysis with the IBDV polyprotein containing the capsid precursor polypeptide has recently shown that VPX has a preferential cleavage site, but another three alternative cleavage sites can be used in the ^{485}A-to-A^{513} stretch (43, 70). This processing is carried out by VP4, but further processing to VP2 is carried out by an unknown mechanism. Since VP2 does not accumulate intracellularly, as the other proteins do, posttranslational modification of VPX into VP2 probably occurs during or after virus assembly (59). Recent data indicate that IBDV assembly is coupled with polyprotein cleavage in a cleavage rate-restricted manner (7). The VP4 protease would be a key regulator, and it is possible that VP3 could provide additional information required to ensure the fidelity of the process, together with its role in providing structural integrity to the IBDV capsid.

Small VP2 capsid as a vaccine. VP2 contains the antigenic region responsible for induction of neutralizing antibodies (2, 6). The self-assembled small VP2 capsids show a topography similar to that of infectious virions, as both expose the upper domain of VP2 in the protruding trimeric units. Therefore, small VP2 particles should mimic conformational epitopes of intact IBDV virions, and their immunogenicity may be similar to that of infectious virions. This small VP2 capsid might be considered as a candidate for serological tests instead of whole virions, and it also provides a starting point in the design of alternatives to live IBDV vaccines for prevention of infectious bursal disease.

Conclusions. Although the similarities between dsRNA viruses at structural and functional levels are well established, there must be profound differences during the life cycle of IBDV, particularly in viral assembly and replication mechanisms. The C terminus of the IBDV VPX region plays a critical role in viral assembly. Its hydrophobic character is almost certainly required for the molecular switching mechanism. The plasticity of VP2, in part due to putative progressive proteolytic processing of its own C-terminal portion, is revealed as an important factor. Our results show a polymorphism in the assembly of a single capsid protein that allows in vivo assembly of 60 VP2 subunits in equivalent environments or of 780 VP2 subunits in five nonequivalent environments. However, VP3 would act to restrict the flexibility of VP2 and is an essential structural component for the proper assembly of VP2 into a T=13 capsid.

ACKNOWLEDGMENTS

The continuous support of A. C. Steven and B. L. Trus (NIH) during the implementation of these procedures in our laboratory is deeply appreciated. We are pleased to acknowledge T. S. Baker (Purdue University, West Lafayette, Ind.) for sharing his reconstruction software, B. L. Trus for providing the PIC system, R. W. Crowther (MRC, Cambridge, United Kingdom) for kindly providing the "facets" program, J. F. Conway (Grenoble, France), D. Belnap (NIH), and R. Ashmore (Purdue University) for assistance in running programs, L. G. de la Fraga (Mexico D.F., Mexico) and J. J. Fernández (Málaga, Spain) for software development, P. Moutel (CSIC) and T. Dinh-Phung and P. Hill (NIH) for assistance in setting up the computers, M. Cerritelli (NIH) for the gift of T4 bacteriophage, and L. Sánchez-Pulido (CNB) for VP2 secondary-structure prediction. We are also indebted to all of them and to O. Llorca (London, United Kingdom) and S. Marco (Tours, France) for stimulating discussions and helpful hints. We gratefully acknowledge the use of the Philips CM12 electron microscope at the Laboratoire des Protéines Complexes (Université Francois Rabelois, Tours, France).

This work was partly supported by grant PB96-0818 from the Dirección General de Investigación Científica y Técnica and by grants 09/038/1997 and 07B/032/1998 from the Comunidad Autónoma de Madrid. J.R.C. holds a postdoctoral contract from the M.E.C., and A.M. is a Fellow at the CICYT.

REFERENCES

1. **Al-Khayat, H. A., D. Bhella, J. M. Kenney, J.-F. Roth, A. J. Kingsman, E. Martin-Rendon, and H. R. Saibil.** 1999. Yeast Ty retrotransposons assemble into virus-like particles whose T-numbers depend on the C-terminal length of the capsid protein. J. Mol. Biol. **292:**65–73.
2. **Azad, A. A., M. N. Jagadish, M. A. Brown, and P. J. Hudson.** 1987. Deletion mapping and expression in *Escherichia coli* of the large genomic segment of a birnavirus. Virology **161:**145–152.
3. **Baker, T. S., and R. H. Cheng.** 1996. A model-based approach for determining orientations of biological macromolecules imaged by cryoelectron microscopy. J. Struct. Biol. **116:**120–130.
4. **Baker, T. S., J. Drak, and M. Bina.** 1988. Reconstruction of the three-dimensional structure of simian virus 40 and visualization of the chromatin core. Proc. Natl. Acad. Sci. USA **85:**422–426.
5. **Baker, T. S., N. H. Olson, and S. D. Fuller.** 1999. Adding the third dimension to virus life cycles: three-dimensional reconstructions of icosahedral viruses from cryoelectron micrographs. Microbiol. Mol. Biol. Rev. **63:**862–922.
6. **Becht, H., H. Müller, and H. K. Müller.** 1988. Comparative studies on structural and antigenic properties of two serotypes of infectious bursal disease virus. J. Gen. Virol. **69:**631–640.
7. **Birghan, C., E. Mundt, and A. E. Gorbalenya.** 2000. A non-canonical lon proteinase lacking the ATPase domain employs the Ser-Lys catalytic dyad to exercise broad control over the life cycle of a double-stranded RNA virus. EMBO J. **19:**114–123.

8. **Böttcher, B., N. A. Kiselev, V. Y. Stel'Mashchuk, N. A. Perevozchikova, A. V. Borisov, and R. A. Crowther.** 1997. Three-dimensional structure of infectious bursal disease virus determined by electron cryomicroscopy. J. Virol. **71:**325–330.
9. **Burroughs, J. N., R. S. O'Hara, C. J. Smale, C. Hamblin, A. Walton, R. Armstrong, and P. P. C. Mertens.** 1994. Purification and properties of virus particles, infectious subviral particles, cores and VP7 crystals of African horsesickness virus serotype 9. J. Gen. Virol. **75:**1849–1857.
10. **Butcher, S. J., T. Dokland, P. M. Ojala, D. H. Bamford, and S. D. Fuller.** 1997. Intermediates in the assembly pathway of the double-stranded RNA virus ϕ6. EMBO J. **16:**4477–4487.
11. **Caspar, D. L. D., and A. Klug.** 1962. Physical principles in the construction of regular viruses. Cold Spring Harbor Symp. Quant. Biol. **27:**1–24.
12. **Castón, J. R., B. L. Trus, F. P. Booy, R. B. Wickner, J. S. Wall, and A. C. Steven.** 1997. Structure of L-A virus: a specialized compartment for the transcription and replication of double-stranded RNA. J. Cell Biol. **138:**975–985.
13. **Cheng, R. H., J. R. Castón, G. Wang, F. Gu, T. J. Smith, T. S. Baker, R. F. Bozarth, B. L. Trus, N. Cheng, R. B. Wickner, and A. C. Steven.** 1994. Fungal virus capsids: cytoplasmic compartments for the replication of double-stranded RNA formed as icosahedral shells of asymmetric Gag dimers. J. Mol. Biol. **244:**255–258.
14. **Conway, J. F., B. L. Trus, F. P. Booy, W. W. Newcomb, J. C. Brown, and A. C. Steven.** 1993. The effects of radiation damage on the structure of frozen hydrated HSV-1 capsids. J. Struct. Biol. **111:**222–233.
15. **Crowther, R. A.** 1971. Procedures for three-dimensional reconstruction of spherical viruses by Fourier synthesis from electron micrographs. Phil. Trans. R. Soc. Ser. B **261:**221–230.
16. **Crowther, R. A., D. J. DeRosier, and A. Klug.** 1970. The reconstruction of a three-dimensional structure from projections and its applications to electron microscopy. Proc. R. Soc. Lond. A **317:**319–340.
17. **de Haas, F., A. O. Paatero, L. Mindich, D. H. Bamford, and S. D. Fuller.** 1999. A symmetry mismatch at the site of RNA packaging in the polymerase complex of dsRNA bacteriophage ϕ6. J. Mol. Biol. **294:**357–372.
18. **Dobos, P., B. J. Hill, R. Hallett, D. T. C. Kells, H. Becht, and D. Teningess.** 1979. Biophysical and biochemical characterization of five animal viruses with bisegmented double-stranded RNA genomes. J. Virol. **32:**593–605.
19. **Dokland, T.** 2000. Freedom and restraint: themes in virus capsid assembly. Structure **8:**R157–R162.
20. **Dryden, K. A., G. Wang, M. Yeager, M. L. Nibert, K. M. Coombs, D. B. Furlong, B. N. Fields, and T. S. Baker.** 1993. Early steps in reovirus infection are associated with dramatic changes in supramolecular structure and protein conformation: analysis of virions and subviral particles by cryoelectron microscopy and image reconstruction. J. Cell Biol. **122:**1023–1041.
21. **Dubochet, J., M. Adrian, J. J. Chang, J. C. Homo, J. Lepault, A. W. McDowall, and P. Schultz.** 1988. Cryo-electron microscopy of vitrified specimens. Q. Rev. Biophys. **21:**129–228.
22. **Fahey, K. J., I. J. O'Donnell, and A. A. Azad.** 1985. Characterization by Western blotting of the immunogens of infectious bursal disease virus. J. Gen. Virol. **66:**1479–1488.
23. **Fahey, K. J., K. Erny, and J. Crooks.** 1989. A conformational immunogen on VP-2 of infectious bursal disease virus that induces virus-neutralizing antibodies that passively protect chickens. J. Gen. Virol. **70:**1473–1481.
24. **Fernández-Arias, A., C. Risco, S. Martínez, J. P. Albar, and J. F. Rodríguez.** 1998. Expression of ORF A1 of infectious bursal disease virus results in the formation of virus-like particles. J. Gen. Virol. **79:**1047–1054.
25. **Fuller, S. D.** 1987. The T=4 envelope of Sindbis virus is organized by interactions with a complementary T=3 capsid. Cell **48:**923–934.
26. **Fuller, S. D., S. J. Butcher, R. H. Cheng, and T. S. Baker.** 1996. Three-dimensional reconstruction of icosahedral particles—the uncommon line. J. Struct. Biol. **116:**48–55.
27. **Gardner, H., K. Kerry, M. Riddle, S. Brouwer, and L. Gleeson.** 1997. Poultry virus infection in Antarctic penguins. Nature **387:**245.
28. **Granzow, H., C. Birgham, T. C. Mettenleiter, J. Beyer, B. Köllner, and E. Mundt.** 1997. A second form of infectious bursal disease virus-associated tubule contains VP4. J. Virol. **71:**8879–8885.
29. **Grimes, J., A. K. Basak, P. Roy, and D. I. Stuart.** 1995. The crystal structure of bluetongue virus VP7. Nature **373:**167–170.
30. **Grimes, J. M., J. N. Burroughs, P. Gouet, J. M. Diprose, R. Malby, S. Ziéntaras, P. P. C. Mertens, and D. I. Stuart.** 1998. The atomic structure of the bluetongue virus core. Nature **395:**470–478.
31. **Grimes, J. M., J. Jakana, M. Ghosh, A. K. Basak, P. Roy, W. Chiu, D. I. Stuart, and B. V. B. Prasad.** 1997. An atomic model of the outer layer of the bluetongue virus core derived from X-ray crystallography and electron cryomicroscopy. Structure **5:**885–893.
32. **Hewat, E. A., T. F. Booth, P. T. Loudon, and P. Roy.** 1992. Three-dimensional reconstruction of baculovirus expressed bluetongue virus core-like particles by cryo-electron microscopy. Virology **189:**10–20.
33. **Hill, C. L., T. F. Booth, B. V. B. Prasad, J. M. Grimes, P. C. Mertens, G. C. Sutton, and D. I. Stuart.** 1999. The structure of a cypovirus and the functional organization of dsRNA viruses. Nat. Struct. Biol. **6:**565–568.
34. **Hsu, G. G., A. R. Bellamy, and M. Yeager.** 1997. Projection structure of VP6, the rotavirus inner capsid protein, and comparison with bluetongue VP7. J. Mol. Biol. **272:**362–368.
35. **Hudson, P. J., N. M. McKern, B. E. Power, and A. A. Azad.** 1986. Genomic structure of the large RNA segment of infectious bursal disease virus. Nucleic Acids Res. **14:**5001–5012.
36. **Johnson, J. E.** 1996. Functional implications of protein-protein interactions in icosahedral viruses. Proc. Natl. Acad. Sci. USA **93:**27–33.
37. **Johnson, J. E., and J. A. Speir.** 1997. Quasi-equivalent viruses: a paradigm for protein assemblies. J. Mol. Biol. **269:**665–675.
38. **Kibenge, F. S. B., A. S. Bhillon, and R. G. Russell.** 1988. Biochemistry and immunology of infectious bursal disease virus. J. Gen. Virol. **69:**1757–1775.
39. **Kitts, P. A., and R. D. Possee.** 1993. A method for producing recombinant baculovirus expression vectors at high frequency. BioTechniques **14:**810–817.
40. **Krol, M. A., N. H. Olson, J. Tate, J. E. Johnson, T. S. Baker, and P. Ahlquist.** 1999. RNA-controlled polymorphism in the in vivo assembly of 180-subunit and 120-subunit virions from a single capsid protein. Proc. Natl. Acad. Sci. USA **96:**13650–13655.
41. **Lawton, J. A., M. K. Estes, and B. V. V. Prasad.** 2000. Mechanism of genome transcription in segmented dsRNA viruses. Adv. Virus Res. **55:**185–229.
42. **Lawton, J. A., C. Q.-Y. Zeng, S. K. Mukherjee, J. Cohen, M. K. Estes, and B. V. B. Prasad.** 1997. Three-dimensional structural analysis of recombinant rotavirus-like particles with intact and amino-terminal-deleted VP2: implications for the architecture of the VP2 capsid layer. J. Virol. **71:**7353–7360.
43. **Lejal, N., B. Da Costa, J.-C. Huet, and B. Delmas.** 2000. Role of Ser-652 and Lys-692 in the protease activity of infectious bursal disease virus VP4 and identification of its substrate cleavage sites. J. Gen. Virol. **81:**983–992.
44. **Leong, J. C., D. Brown, P. Dobos, F. S. B. Kibenge, J. E. Ludert, H. Muller, E. Mundt, and B. Nicholson.** 2000. Family *Birnaviridae*, p. 481–490. *In* M. H. V. van Regenmortel, C. M. Fauquet, D. H. L. Bishop, E. B. Carstens, M. K. Estes, S. M. Lemon, J. Maniloff, M. A. Mayo, D. J. McGeoch, C. R. Pringle, and R. B. Wickner (ed.), Virus taxonomy: classification and nomenclature of viruses. Seventh report of the International Committee on Taxonomy of Viruses. Academic Press, San Diego, Calif.
45. **Lepault, J., and K. Leonard.** 1985. Three-dimensional structure of unstained, frozen-hydrated extended tails of bacteriophage T4. J. Mol. Biol. **182:**431–441.
46. **Lepault, J., I. Petitpas, I. Erk, J. Navaza, D. Bigot, M. Dona, P. Vachette, J. Cohen, and F. A. Rey.** 2001. Structural polymorphism of the major capsid protein of rotavirus. EMBO J. **20:**1498–1507.
47. **Liddington, R. C., Y. Yan, J. Moulai, R. Sahli, T. L. Benjamin, and S. C. Harrison.** 1991. Structure of simian virus 40 at 3.8 Å resolution. Nature **354:**278–284.
48. **Lombardo, E., A. Maraver, J. R. Castón, J. Rivera, A. Fernández-Arias, A. Serrano, J. L. Carrascosa, and J. F. Rodríguez.** 1999. VP1, the putative RNA-dependent RNA polymerase of infectious bursal disease virus, forms complexes with the capsid protein VP3, leading to efficient encapsidation into virus-like particles. J. Virol. **73:**6973–6983.
49. **Lombardo, E., A. Maraver, I. Espinosa, A. Fernández-Arias, and J. F. Rodríguez.** 2000. VP5, the nonstructural polypeptide of infectious bursal disease virus, accumulates within the host plasma membrane and induces cell lysis. Virology **277:**345–357.
50. **Lu, G., Z. H. Zhou, M. L. Baker, J. Jakana, D. Cai, X. Wei, S. Chen, X. Gu, and W. Chiu.** 1998. Structure of double-shelled rice dwarf virus. J. Virol. **72:**8541–8549.
51. **Martínez-Torrecuadrada, J. L. M., J. R. Castón, M. Castro, J. L. Carrascosa, J. F. Rodríguez, and J. I. Casal.** 2000. Different architectures in the assembly of infectious bursal disease virus capsid proteins expressed in insect cells. Virology **278:**322–331.
52. **Martínez-Torrecuadrada, J. L. M., B. Lázaro, J. F. Rodríguez, and J. I. Casal.** 2000. Antigenic properties and diagnostic potential of baculovirus-expressed infectious bursal disease virus proteins VPX and VP3. Clin. Diagn. Lab. Immunol. **7:**645–651.
53. **Mathieu, M., I. Petitpas, J. Navaza, J. Lepault, E. Kohli, P. Pothier, B. V. V. Prasad, J. Cohen, and F. A. Rey.** 2001. Atomic structure of the major capsid protein of rotavirus: implications for the architecture of the virion. EMBO J. **20:**1485–1497.
54. **Matsumura, Y., R. D. Possee, H. A. Overton, and D. H. L. Bishop.** 1987. Baculovirus expression vectors: the requirements for high level expression of proteins, including glycoproteins. J. Gen. Virol. **68:**1233–1250.
55. **Metcalf, P., M. Cyrklaff, and M. Adrian.** 1991. The three-dimensional structure of reovirus by cryo-electron microscopy. EMBO J. **10:**3129–3136.
56. **Mindich, M., and D. H. Bamford.** 1988. Lipid-containing bacteriophages, p. 475–520. *In* R. Calendar (ed.), The bacteriophages, vol. 2. Plenum Press, New York, N.Y.
57. **Moody, M. F., and L. Makowski.** 1981. X-ray diffraction study of tail-tubes from bacteriophage T2L. J. Mol. Biol. **150:**217–244.
58. **Morgan, M. M., I. G. Macreadie, V. R. Harley, P. J. Hudson, and A. A. Azad.** 1988. Sequence of the small double-stranded RNA genomic segment of infectious bursal disease virus and its deduced 90-kDa product. Virology **163:**240–242.
59. **Müller, H., and H. Becht.** 1982. Biosynthesis of virus-specific proteins in cells infected with infectious bursal disease virus and their significance as struc-

tural elements for infectious virus and incomplete particles. J. Virol. **44:**384–392.
60. **Mundt, E., B. Köllner, and D. Kretzschmar.** 1997. VP5 of infectious bursal disease virus is not essential for virus replication in cell culture. J. Virol. **71:**5647–5651.
61. **Nagarajan, M. M., and F. S. B. Kibenge.** 1995. Infectious bursal disease virus: a review of molecular basis for variations in antigenicity and virulence. Can. J. Vet. Res. **61:**81–88.
62. **Nason, E. L., S. K. Samal, and B. V. V. Prasad.** 2000. Trypsin-induced structural transformation in aquareovirus. J. Virol. **74:**6546–6555.
63. **Petitpas, I., J. Lepault, P. Vachette, A. Charpilienne, M. Mathieu, E. Kohli, P. Pothier, J. Cohen, and F. A. Rey.** 1998. Crystallization and preliminary X-ray analysis of rotavirus protein VP6. J. Virol. **72:**7615–7619.
64. **Prasad, B. V. V., R. Rothnagel, C. Q.-Y. Zeng, J. Jakana, J. A. Lawton, W. Chiu, and M. K. Estes.** 1996. Visualization of ordered genomic RNA and localization of transcriptional complexes in rotavirus. Nature **382:**471–473.
65. **Prasad, B. V. V., G. J. Wang, J. P. M. Clerx, and W. Chiu.** 1988. Three-dimensional structure of rotavirus. J. Mol. Biol. **199:**269–275.
66. **Prasad, B. V. V., S. Yamaguchi, and P. Roy.** 1992. Three-dimensional structure of single-shelled bluetongue virus. J. Virol. **66:**2135–2142.
67. **Radermacher, M.** 1992. Weighted back-projection methods, p. 91–115. *In* J. Frank (ed.), Electron tomography: three-dimensional imaging with the transmission electron microscope. Plenum, New York, N.Y.
68. **Reinisch, K. M., M. L. Nibert, and S. C. Harrison.** 2000. Structure of the reovirus core at 3.6 Å resolution. Nature **404:**960–967.
69. **Rossmann, M. G., and J. E. Johnson.** 1989. Icosahedral RNA virus structure. Annu. Rev. Biochem. **58:**533–573.
70. **Sánchez, A. B., and J. F. Rodríguez.** 1999. Proteolytic processing in infectious bursal disease virus: identification of the polyprotein cleavage sites by site-directed mutagenesis. Virology **262:**190–199.
71. **Saxton, W. O., and W. Baumeister.** 1982. The correlation averaging of a regularly arranged bacterial cell envelope protein. J. Microsc. **127:**127–138.
72. **Shaw, A. L., S. K. Samal, K. Subramanian, and B. V. V. Prasad.** 1996. The structure of aquareovirus shows how the different geometries of the two layers of the capsid are reconciled to provide symmetrical interactions and stabilization. Structure **4:**957–967.
73. **Spies, U., H. Müller, and H. Becht.** 1987. Properties of RNA polymerase activity associated with infectious bursal disease virus and characterization of its reaction products. Virus Res. **8:**127–140.
74. **Steven, A. C., B. L. Trus, F. P. Booy, N. Cheng, A. Zlotnick, J. R. Castón, and J. F. Conway.** 1997. The making and breaking of symmetry in virus capsid assembly: glimpses of capsid biology from cryoelectron microscopy. FASEB J. **11:**733–742.
75. **Tacken, M. G. J., P. J. M. Rottier, A. L. J. Gielkens, and B. P. H. Peeters.** 2000. Interactions *in vivo* between the proteins of infectious bursal disease virus: capsid protein VP3 interacts with the RNA-dependent RNA polymerase, VP1. J. Gen. Virol. **81:**209–218.
76. **Trus, B. L., E. Kocsis, J. F. Conway, and A. C. Steven.** 1996. Digital image processing of electron micrographs: the PIC system-III. J. Struct. Biol. **116:**61–67.
77. **van den Berg, T. P.** 2000. Acute infectious bursal disease in poultry: a review. Avian Pathol. **29:**175–194.
78. **Wickner, R. B.** 1996. Double-stranded RNA viruses of *Saccharomyces cerevisiae*. Microbiol. Rev. **60:**250–265.
79. **Yeager, M., K. A. Dryden, N. H. Olson, H. B. Greenberg, and T. S. Baker.** 1990. Three-dimensional structure of rhesus rotavirus by cryoelectron microscopy and image reconstruction. J. Cell Biol. **110:**2133–2144.
80. **Zhang, H., J. Zhang, X. Yu, Q. Zhang, J. Jakana, D. H. Chen, X. Zhang, and Z. H. Zhou.** 1999. Visualization of protein-RNA interactions in cytoplasmic polyhedrosis virus. J. Virol. **73:**1624–1629.
81. **Zhu, Y., A. M. Hemmings, K. Iwasaki, Y. Fujiyoshi, B. Zhong, J. Yan, M. Isogai, and T. Omura.** 1997. Details of the arrangement of the outer capsid of rice dwarf phytoreovirus, as visualized by two-dimensional crystallography. J. Virol. **71:**8899–8901.